Tunable thin-film filters: review and perspectives

Michel Lequime

Institut FRESNEL – UMR CNRS 6133
Domaine Universitaire de Saint-Jérôme, 13397 Marseille Cedex 20 – France

ABSTRACT

The development of tunable filters is a key point for the ability of optical telecommunication networks to comply with the continuous evolution of the service providers needs. Among the numerous technologies which can be used to achieve narrow bandpass filtering devices, we concentrate our analysis on Thin-Film Interference Coatings and compare the principles, performances and use constraints of the various schemes allowing to tune such a thin-film structure : tilt of a standard bandpass filter, translation of a linear variable filter, deformation of the substrate of a DWDM filter, implementation of active spacers with controllable optical thickness (thin-films or solid spaced etalons).

Keywords: thin-film filters, tunable optical filters, DWDM, Telecommunication networks

1. INTRODUCTION

Since the early 1990s, the use of wavelength division multiplexing (WDM) has allowed for a dramatic increase in the capacity of telecommunication fiber-optic networks. Current architectures exploit fixed optical filters, which are fabricated with central wavelengths corresponding to the frequencies defined by the ITU grid, i.e. from 186 to 191 THz for the L-Band, from 191 to 196 THz for the C-Band and from 196 to 201 THz for the S-Band, the frequency interval between two adjacent channels being fixed to either 50 or 100 GHz : consequently, the number of optical channels which propagate through the network can be quite large (up to 100 in each Band for the 50 GHz grid), and the manufacture of such optical filters is demanding, essentially because of the different constraints imposed by the use of this dense spectral grid (accuracy and stability of the central wavelength, narrowness of the spectral bandwidth, magnitude of the isolation for the adjacent channels).

The architecture of the system could be considerably simplified and the complexity of the wavelength discriminating components greatly reduced if the optical filters could be provided as frequency agile elements. Tunable optical filters are therefore key components for flexible channel selection and monitoring. Candidate technologies include temperature- or strain-tuned fiber Bragg gratings, cascaded waveguide Mach-Zehnder interferometers with resistive heaters, classical diffraction gratings, volume Bragg gratings array addressed by a mechanical switch, electrostatically driven micro Fabry-Perot cavities structures (MEMS), liquid crystal Fabry-Perot etalons, angle tuned standard narrowband thin-film filters, linear variable thin-film filter addressed by translation, and thin-film filters with active substrates or active layers [1, 2].

The objectives of this paper are to perform a rapid presentation of the different concepts of tunable thin-film filter and to provide with an applicable synthesis including conclusions and perspectives.

2. ANGLE-TUNED THIN-FILM FILTERS

The variation of the performances of an all-dielectric Fabry-Perot with angle of incidence is a well known effect, which has been widely studied [3, 4] and often used by the manufacturers to ease a little some too tight production tolerances. Basically, the tuning equation of such a filter is given by

$$\lambda_\theta = \lambda_0 \sqrt{1-(\sin^2\theta / n_{eff}^2)}$$

where λ_0 (respectively λ_θ) is the center wavelength of the filter at normal incidence (respectively oblique incidence), θ the angle of incidence of the collimated light beam in air and n_{eff} the effective index of refraction of the filter.

This last quantity depends of the nature of the spacers (high- or low-index) of the elementary Fabry-Perot cavities used in the design of our narrowband thin-film filter and varies with m, the interference order of these cavities and n_H and n_L, the refractive indices of the quarter-wave alternated layers used for the realization of their high reflectance mirrors

$$n_{eff} = \begin{cases} n_H \sqrt{\dfrac{m-(m-1)(n_L/n_H)}{(m-1)-(m-1)(n_L/n_H)+(n_H/n_L)}} & \text{for high - index spacers} \\ n_L \sqrt{\dfrac{m-(m-1)(n_L/n_H)}{(m-m(n_L/n_H)+(n_L/n_H)^2}} & \text{for low - index spacers} \end{cases}$$

To reach the maximum tuning range for a given angle of incidence in air, we need to minimize this effective index, i.e. to select preferentially a low-index spacer and a quite high interference order.

Typical curves are given in figure 1 and show how, in this simplified approach, the central wavelength of a 3-cavity SiO_2/Ta_2O_5 thin-film filter centered at 1570 nm varies with the angle of incidence for 4L (m = 2, grey line) and 12L (m = 6, bold line) spacers.

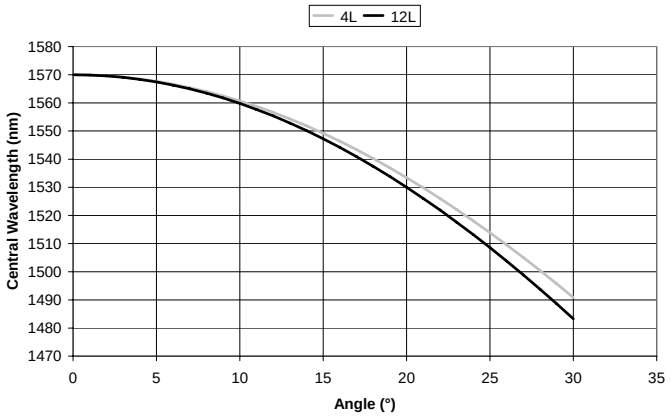

Figure 1 – Shift of the peak wavelength with angle of incidence

However, this very simple approach does not take into account the polarization effects, which induce a splitting of the transmittance curves for S- and P-polarization states, together with a slight narrowing of the filter shape for the S state and a similar broadening for the P state. Figure 2 shows the features of such effects for the previous 4L-spacer 3-cavity filter.

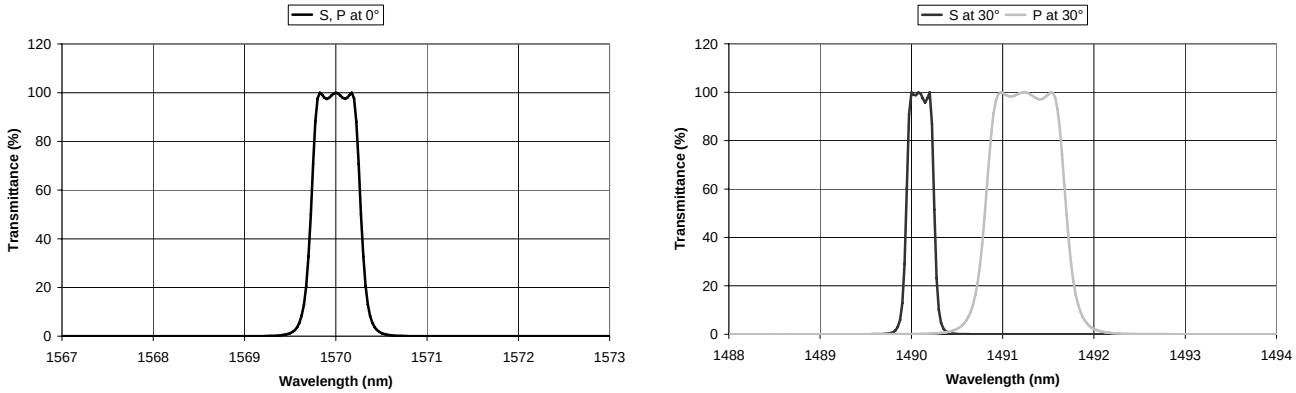

Figure 2 – Polarization effects in angle-tuned standard thin-film filter

We can notice that the use of the previous simplified approach leads to a unique central wavelength about 1491 nm at 30° of incidence, and that the amplitude of the deviation of each polarization state with respect to this prediction is about ± 0.5 nm.

To overcome this divergence of S- and P-polarization bandpasses, we can add diversity optics to our wavelength discriminating component, but the resulting system becomes complex and expensive. Another (and simpler) way is to use layers matched at a given angle of incidence (for instance 20°) in the design of our narrow band-pass filter. This ensures the coincidence of the two central wavelengths at 0° and 20° of incidence and minimizes the shape changes in this whole angular range. An illustration of such a behavior is presented at the figure 3, for a 4L-spacer 3-cavity filter matched at 20° and 1530 nm.

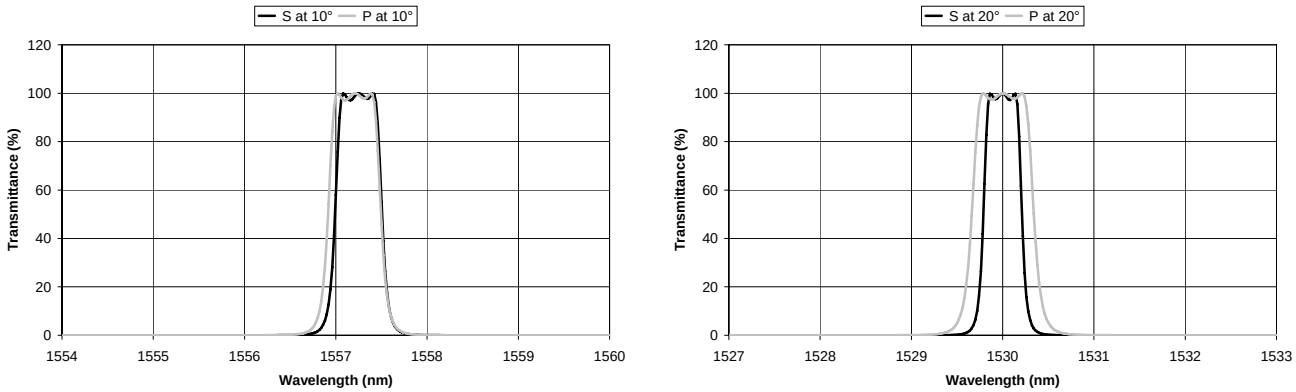

Figure 3 – Polarization effects in angle-tuned matched thin-film filter

Angle-tuned thin-film filters with such improved behavior are commercially proposed for instance by Micron Optics Inc. under the generic name of Chameleon [5].

3. LINEAR SLIDING TUNABLE THIN-FILM FILTERS

The key component of this tuning scheme is a linear variable filter (sometimes also called wedge filter), i.e. an all-dielectric bandpass thin-film filter that has been manufactured with a linear dependence of its layers thickness along one axis [1]. Accordingly, the central wavelength of such wedged thickness coatings changes linearly with the position along its length, while the bandpass remains. Dedicated masking techniques are used in deposition systems (Ion Assisted Deposition or Dual Ion Beam Sputtering) to achieve such a result on rotating substrates [see for instance 6].

The input Gaussian light beam is focused onto the filter surface at a position which corresponds to the selected wavelength. Consequently, the resulting filter shape is broadened because of the finite size of the beam waist along the linearly varying filter direction: this effect incites naturally to use small size waist w_0. But the divergence θ of the beam at the filter surface is inversely proportional to the same waist size ($\theta = \lambda/\pi w_0$), and the shape of the resulting filter is again broadened by the weighted average of the angular responses from 0 to θ. Therefore, the optimum design corresponds to a compromise between these two opposed effects. However, we can notice that the use of high-index spacers and moderate interference order can simplify its definition (see section 2).

This linear sliding tuning method is used for instance by SANTEC Corporation [7] to propose a programmable device which provides with a simultaneous control of wavelength and power through a combination of linear variable filters and attenuators.

4. ACTIVE SUBSTRATES

The basic idea of this indirect tuning scheme is to transfer a mechanical strain of the substrate to the spacer thickness of a standard DWDM bandpass filter deposited at its surface [2] and to achieve consequently a change in the resonant wavelength of this all-dielectric Fabry-Perot structure. This idea comes from a reflection on Takashashi's paper [8] on temperature stability of thin-film narrow bandpass filter. In his paper Takashashi analyzes the opposite effects of two

mechanisms, first the increase of the refractive index of the layers created by a rising temperature and secondly the change of their thickness induced by a differential thermal expansion between the layers and the substrate.

The objective of Takashashi was to reduce the thermal sensitivity of the peak wavelength of a narrow-bandpass filter to less than 1 pm/°C, and this can be achieved by the choice of an appropriate substrate with a coefficient of thermal expansion around 110.10^{-7} /°C. But at the opposite we can aim at amplifying this thermal sensitivity and the choice of the substrate can participate in the fulfillment of this new goal. On the other hand, if the temperature is now kept constant, a mechanical deformation of the substrate, i.e. a strain, can be also used to induce a shift in the design wavelength of this filter: this strain can be produced for instance by a compressive force applied on a standard substrate or by an electric field applied on a piezoelectric substrate.

We will present the different steps of our calculus first in the case of the temperature. The filter assembly is represented at the figure 4, the grey part corresponding to the layers stack and the white one to the substrate. We assume moreover that the all-dielectric thin-film can be replaced by a single layer whose mechanical thickness is equal to the thickness of the stack and whose refractive index is equal to the effective value n_{eff} defined at the Section 2.

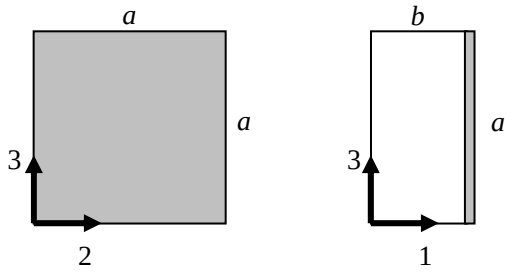

Figure 4 – Schematic representation of a DWDM filter

However, unlike Takashashi, we prefer to adopt a theoretical description based on a direct tensor calculation [9], taking into account the elastic properties of both substrate and filter as well as the elasto-optic coefficients of our equivalent layer: this alternative approach is better adapted to the use of anisotropic substrate and makes it possible to quantify polarization effects. Shearing effects are here neglected.

The effect that we aim at quantifying is produced by the difference between the coefficients of thermal expansion of the substrate (α) and the equivalent layer (β). Consequently, the principal strains of this layer are defined by

$$\varepsilon_1^f ; \varepsilon_2^f ; \varepsilon_3^f \quad \text{with} \quad \varepsilon_2^f = \varepsilon_2^f = (\alpha - \beta) \cdot \Delta T = \varepsilon$$

where ΔT is the temperature change. In the same way, the principal stresses applied to the stack are defined by

$$\sigma_1^f ; \sigma_2^f ; \sigma_3^f \quad \text{with} \quad \sigma_1^f = 0 \quad \text{and} \quad \sigma_2^f = \sigma_3^f = \sigma$$

To find the missing quantities and especially the strain along the 1-axis, we shall combine the previous equations with the elastic-strain relations describing the mechanical behavior of the equivalent layer, i.e.

$$\varepsilon_i^f = \frac{1+\nu_f}{Y_f}\sigma_i^f - \frac{\nu_f}{Y_f}(\sigma_1^f + \sigma_2^f + \sigma_3^f) \quad i = 1, 2, 3$$

where ν_f and Y_f designate respectively the Poisson coefficient of this layer and its Young modulus. We obtain finally

$$\varepsilon_1^f = -\frac{2\nu_f}{1-\nu_f}\varepsilon \quad ; \quad \varepsilon_2^f = \varepsilon \quad ; \quad \varepsilon_3^f = \varepsilon$$

In a first approximation, the relative center wavelength shift $\Delta\lambda/\lambda$ of the DWDM filter is defined by

$$\left.\frac{\Delta\lambda}{\lambda}\right|_i = \frac{\Delta(n_i t_f)}{n_i t_f} = \varepsilon_1^f + \frac{\Delta n_i}{n_i} \quad i = 2, 3$$

where t_f is the thickness of the equivalent layer and i the polarization direction of the incident light beam. Consequently, it is now required to determine the relative change in the refractive indexes Δn_i of the equivalent layer induced by its mechanical deformation (elasto-optic effect). If we assume that this equivalent layer is initially an isotropic and centro-symmetric material, we can write

$$\begin{pmatrix} \Delta(1/n_1^2) \\ \Delta(1/n_2^2) \\ \Delta(1/n_3^2) \end{pmatrix} = -\frac{2}{n_{eff}^2} \begin{pmatrix} \Delta n_1 / n_1 \\ \Delta n_2 / n_2 \\ \Delta n_3 / n_3 \end{pmatrix} = \begin{bmatrix} p_{11} & p_{12} & p_{12} \\ p_{12} & p_{11} & p_{12} \\ p_{12} & p_{12} & p_{11} \end{bmatrix} \begin{pmatrix} \varepsilon_1^f \\ \varepsilon_2^f \\ \varepsilon_3^f \end{pmatrix}$$

where [**p**] is the effective elasto-optic tensor of the stack.

The relative changes in the indexes of refraction induced by the layer strain are

$$\frac{\Delta n_2}{n_2} = \frac{\Delta n_3}{n_3} = -\frac{n_{eff}^2}{2}\left[(1-\nu_f)\,p_{11} + (1-3\nu_f)\,p_{12}\right] \cdot \frac{\varepsilon}{1-\nu_f}$$

By combining this relation with the effects directly caused by the temperature change (thermal dilatation β of the equivalent layer and thermo-optic change in its effective refractive index $1/n.\mathrm{d}n/\mathrm{d}T$), we are able to evaluate the global thermal shift of a standard DWDM filter

$$\frac{1}{\Delta T}\frac{\Delta\lambda}{\lambda} = \frac{1}{n}\frac{dn}{dT} + \beta - \frac{\alpha-\beta}{1-\nu_f}\left\{2\nu_f + \frac{n_{eff}^2}{2}\left[(1-\nu_f)\,p_{11} + (1-3\nu_f)\,p_{12}\right]\right\}$$

If we use the same approach as Takashashi for the choice of the physical properties of our equivalent layer (i.e. those of the fused silica, $[(1/n).(\mathrm{d}n/\mathrm{d}T) = 69\ 10^{-7}/°\mathrm{C}$, $\beta = 5.5\ 10^{-7}/°\mathrm{C}$, $\nu_f = 0.17]$), even for the elasto-optic coefficients ($p_{11} = 0.121$ and $p_{12} = 0.270$), the thermal sensitivity of a 4L-spacer thin-film filter is expected to cancel when the substrate's coefficient of thermal expansion α is around $105\ 10^{-7}/°\mathrm{C}$. This last value is in good agreement with both Takashasi results [8] and glass manufacturers data sheets (see for instance [10]).

As indicated above, we can also try to maximize this thermal sensitivity by choosing a substrate whose strain will amplify the spontaneous thermal response of the layers stack. If we use for instance a transparent glass ceramic material with a negative thermal expansion coefficient ($\alpha = -20\ 10^{-7}/°\mathrm{C}$), such as the NEX-C from OHARA Corporation [11], the calculated thermal sensitivity of our narrow-bandpass filter reaches 15 pm/°C, what is attractive but remains comparable to the value achieved with a standard fused silica substrate (around 10 pm/°C). The right solution actually consists to increase the intrinsic thermal sensitivity of the layers stack itself (see Section 5).

Our model being then validated, we can apply it to the description of alternative configurations, like the use of a piezoelectric substrate or the application of a compressive stress.

A schematic representation of a tunable thin-film filter using an active piezoelectric substrate is given at the figure 5. The layers stack is deposited at the top of the substrate (23-plane) and two opposed lateral faces of the same substrate (12-plane) are equipped with thin conductive electrodes connected to a voltage source, in order to produce an uniform electric field E aligned with the 3-axis inside the substrate.

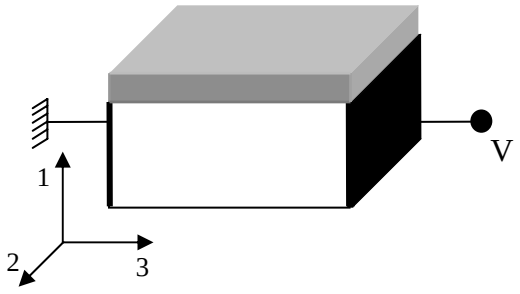

Figure 5 – Schematic representation of a tunable thin-film filter using a piezoelectric substrate

The principal strains of the substrate can be defined with the help of its piezoelectric tensor [**d**]. In our case, we have

$$\varepsilon_1^s = d_{31}E \quad ; \quad \varepsilon_2^s = d_{32}E \quad ; \quad \varepsilon_3^s = d_{33}E$$

Let us assume that the strain of the substrate is integrally transferred to the stack (i.e. at the equivalent layer) in the 23-plane (perfect adhesion hypothesis).

The use of the elastic-strain relations describing the mechanical behavior of the equivalent layer leads to

$$\varepsilon_2^f = d_{32}E \quad ; \quad \varepsilon_3^f = d_{33}E \quad ; \quad \varepsilon_1^f = -\frac{\nu_f}{1-\nu_f}(\varepsilon_2^f + \varepsilon_3^f) = -\frac{\nu_f}{1-\nu_f}(d_{32} + d_{33})E$$

By using the same approach as previously described for the temperature, we are able to evaluate the elasto-optic refractive index changes, then the relative shift of the central wavelength of the filter for both polarization states

$$\left.\frac{\Delta\lambda}{\lambda}\right|_2 = -\frac{1}{1-\nu_f}\left\{\nu_f(d_{32}+d_{33}) + \frac{n_{eff}^2}{2}\left(d_{32}[(1-\nu_f)p_{11} - \nu_f p_{12}] + d_{33}p_{12}[1-2\nu_f]\right)\right\}\cdot E$$

$$\left.\frac{\Delta\lambda}{\lambda}\right|_3 = -\frac{1}{1-\nu_f}\left\{\nu_f(d_{32}+d_{33}) + \frac{n_{eff}^2}{2}\left(d_{33}[(1-\nu_f)p_{11} - \nu_f p_{12}] + d_{32}p_{12}[1-2\nu_f]\right)\right\}\cdot E$$

Several optical materials present piezoelectric activity (such as quartz, barium titanate, lithium niobate, zinc oxide), but we must obviously select a material that is transparent in the telecommunication band and whose piezoelectric coefficients are as large as possible. With respect to both criteria, barium titanate seems the most promising candidate. For this material, we have [12]: d_{32} = -32.5 pm/V; d_{33} = 90 pm/V. The electric field E shall naturally remain below the breakdown voltage of the material, which is around 10^7 V/m. For such a voltage limit, the spectral shift reaches respectively –0.5 nm for the polarization 2 and –0.15 nm for the polarization 3, what is relatively small.

We can consider alternative materials with larger piezoelectric activity, like the PZT (Lead Zirconate Titanate), but the optical transmittance of this ceramic is too small to be used as DWDM filter substrate. However, we can, with a piezoelectric PZT stack, apply a large compressive force on one of the lateral faces of a standard substrate (see figure 6).

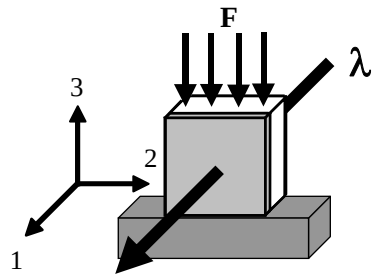

Figure 6 – Schematic representation of a DWDM filter whose substrate is loaded with a uniform uniaxial force

The principal strains of the substrate are defined by (direct application of the elastic-strain relations)

$$\varepsilon_3^s = \frac{F}{abY_s} \quad ; \quad \varepsilon_1^s = \varepsilon_2^s = -\nu_s\varepsilon_3^s$$

where ν_s and Y_s designates respectively the Poisson coefficient of the substrate and its Young modulus. By using the same perfect adhesion hypothesis as for the piezoelectric substrate, we are able to evaluate the principal strains of the equivalent layer

$$\varepsilon_1^f = -\frac{1-\nu_s}{1-\nu_f}\nu_f\varepsilon_3^s \quad ; \quad \varepsilon_2^f = -\nu_s\varepsilon_3^s \quad ; \quad \varepsilon_3^f = \varepsilon_3^s$$

then the relative spectral shift of the central wavelength of the filter for both polarization states 2 and 3

$$\left.\frac{\Delta\lambda}{\lambda}\right|_2 = -\frac{1-\nu_s}{1-\nu_f}\left\{\nu_f + \frac{n_{eff}^2}{2}\left[\frac{1-\nu_f}{1-\nu_s}(p_{12}-\nu_s p_{11}) - \nu_f p_{12}\right]\right\}\cdot\frac{F}{abY_s}$$

$$\left.\frac{\Delta\lambda}{\lambda}\right|_3 = -\frac{1-\nu_s}{1-\nu_f}\left\{\nu_f + \frac{n_{eff}^2}{2}\left[\frac{1-\nu_f}{1-\nu_s}(p_{11}-\nu_s p_{12}) - \nu_f p_{12}\right]\right\}\cdot\frac{F}{abY_s}$$

Let us consider a 4L-spacer filter with standard dimensions (a = 1.4 mm, b = 0.8 mm) and substrate mechanical properties (ν_s = 0.25, Y_s = 78 GPa) : the calculated sensitivity of its design wavelength with respect to the applied force depends on the polarization state and reaches respectively 7 pm/N for the 2-axis and 3 pm/N for the 3 axis.

Experimental confirmation of this effect has been achieved on a classic 200-GHz thin-film filter centered at 1549.32 nm (Full Width at Half Maximum FWHM 1.4 nm) for a light beam polarized along the 2 axis [9]. When a compressive force is applied to the filter substrate, we observe, as expected, a shift of the central wavelength of the filter towards larger wavelengths (a compressive force is negative). The shift value is proportional to the applied force (see figure 7), but the experimental slope is slightly less than theoretically predicted (4.2 pm/N instead of 7 pm/N).

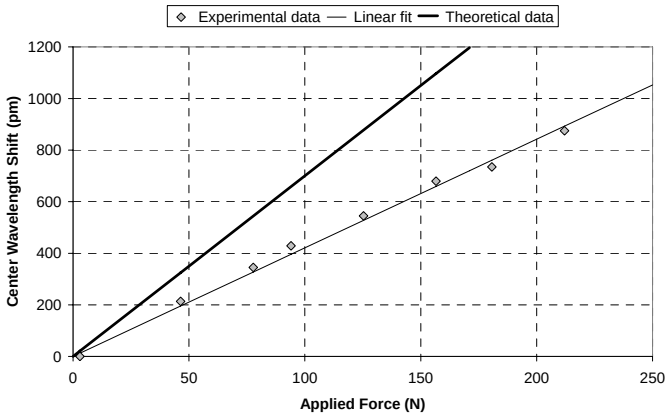

Figure 7 – Center wavelength shift with respect to the applied force

This means that a tuning range around 5 nm can be achieved with a stress below the compressive breaking point of the substrate (typically 1.1 GPa, which here means ~ 1000 N). But such a loading will induce also a large splitting of the transmittance curves for the S- and P-polarization states. To avoid the use of complex and expensive diversity optics, we need only to make isotropic the strain field in the 23-plane, as for the temperature: that can be achieved by adding a second compressive force, identical to the first one, but aligned with the 2–axis. In such a case, the theoretical sensitivity provided by our model is

$$\left.\frac{\Delta\lambda}{\lambda}\right|_2 = \left.\frac{\Delta\lambda}{\lambda}\right|_3 = -\frac{1}{1-\nu_f}\left\{2\nu_f + \frac{n_{eff}^2}{2}\left[(1-\nu_f)p_{11} + (1-3\nu_f)p_{12}\right]\right\}\cdot\frac{F}{abY_s}$$

what leads to a sensitivity around 14 pm/N, without polarization effects.

To achieve such isotropy of the loading, we can easily explore various designs, either by gluing the edge of a standard DWDM filter onto a ring-shaped ceramic or by using special DWDM filter with disk-shaped substrate inserted into a ring-shaped ceramic (the compressive force being applied directly or through a thin glue layer).

5. ACTIVE SPACERS

The basic idea of this last tuning scheme is to act directly on the optical thickness of the spacer of an all-dielectric Fabry-Perot cavity filter by varying the value of a physical parameter around the stack, like the electric field (piezoelectric effect, electro-optic effect) or the temperature (thermo-optic effect). According to the structure of the optical interference coating, this change can affect only the spacer, or only all the high index-layers (for instance) or the whole stack. The relation between the relative spectral shift of the design wavelength of the filter λ_0 and the relative variation of the

optical thickness of the spacer nt_{sp} depends on this condition and can be described in a general way by the following relation [2]

$$\frac{\Delta\lambda}{\lambda_0} = \kappa \frac{\Delta(nt_{sp})}{nt_{sp}}$$

where κ is a positive coefficient, smaller than 1, whose exact value is connected to the structure of the filter and the location of the active layers into the stack. It shall be emphasized that this coefficient increases with the interference order of the elementary Fabry-Perot cavities (for instance $\kappa = 0.87$ for a $[(HL)^6 – 32H – (LH)^6]$ single-cavity structure with active spacer only), and is naturally equal to 1 for any filter design when all the layers are active with the same relative sensitivity.

Active materials can be roughly classified in two groups [13]: the high speed materials with small optical thickness modulations ($\Delta n/n$ or $\Delta t_{sp}/ t_{sp}$ less than 1 ‰) and the low speed materials with larger index modulations ($\Delta n/n$ comprised between 1 ‰ and 1 %). The first group includes the electro-optic crystals, the piezoelectric crystals and the semiconductors (charge injection mechanism), while the second is mainly represented by the liquid crystals, the polymers and again the semiconductors (thermo-optic effect).

We have reported in a previous paper [14] some experimental results on the piezoelectric properties of Ta_2O_5 deposited at high temperature by classic electron-beam evaporation. The use of a substrate heating at 620°C (front side with halogen lamps, rear side through a resistive heater) has allowed us to obtain polycrystalline tantalum pentoxide layers, mainly organized in the orthorhombic (2 0 0) phase, and presenting a noticeable piezoelectric activity (typically 10 pm/V). Such a feature could allow us to achieve a spectral shift of 0.1 nm if we restrict the applied electric field to less than half of the breakdown limit (i.e., 5 kV/mm). Moreover, these polycrystalline layers are characterized by a relatively high refractive index (typically 2.3 @ 633 nm, compared to 2.15 for classical Ta_2O_5 thin-films deposited at ambient temperature), but above all, by high scattering losses induced by their polycrystalline microstructure. The figure 8 shows the BRDF data (Bi-directional Reflectance Distribution Function) recorded on a classical tantalum pentoxide layer deposited by ion assisted electron beam evaporation (IAD, grey line) and on an active layer (T_s = 620°C, bold line): the scattering level is clearly increased by a factor comprised between 50 and 100.

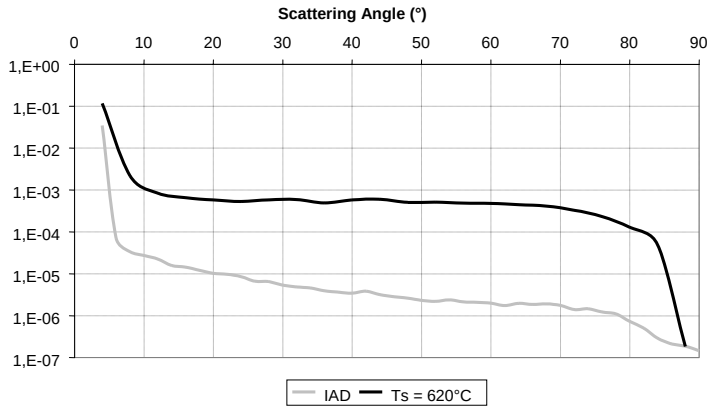

Figure 8 – BRDF data of classical and active Ta_2O_5 layers

The interest in use of such active thin-film layers to produce tunable narrow-bandpass filters is then clearly limited (because of these low tuning range and high scattering losses) and this kind of conclusion can be extended to most of the active high speed materials defined above, if they are achieved through standard thin-film evaporation process.

Of course, this conclusion does not remain completely valid, if the active spacer is achieved by thinning of a bulk crystal plate (final thickness comprised between 20 and 100 microns) and coated with all-dielectric mirrors on its both faces. The use of such solid-spaced etalons in a cascaded configuration enables to eliminate the unwanted transmission peaks which appear around the design wavelength in this manufacturing scheme [15]. Preliminary results have been obtained

experimentally by our team on a solid-spaced $LiNbO_3$ etalon [16], driven through thin deposited ITO electrodes. The sensitivity with respect to the electric field is constant on a large frequency range (from DC to 50 kHz), but the associated tuning range remains quite small (typically less than 1 nm). Replacement of $LiNbO_3$ by $BaTiO_3$ could increase this figure, but the barium titanate remains today a material whose polishing is complex and the use inside an evaporation process delicate.

What happens practically in the case of the second group, i.e. the low-speed materials? AEGIS Semiconductor has recently presented tunable [17] and switchable [18] components using thermo-optic effect in semiconductor thin-films. Active spacers are made of hydrogenated amorphous silicon (a-SI:H) manufactured by Plasma Enhanced Chemical Vapor Deposition (PECVD), while the high reflectance mirrors are alternated quarter-wave layers of silicon nitride (n = 1.77, $k = 10^{-6}$ @ 1550 nm) and hydrogenated amorphous silicon (n = 3.73, $k = 4\ 10^{-6}$ @ 1550 nm). The strong index ratio and the low absorption of the stack layers enable to reach ultra-low (less than 0.1 nm) bandwidth with a relatively small number of layers. However, even if the thermo-optic coefficient of the spacer is unusually large ($dn/dT = 3.6\ 10^{-4}$ /°C), the covering of the C or L bands require filter temperature changes around 350°C and hence extremely robust film adhesion and stability. The temperature changes can be achieved either through transparent conducting heater films or with compact temperature controller, while the manufacturing procedures developed by AEGIS enable the use of so large temperature excursions without MTBF problem (prototype filters have been tested on more than 75 millions cycles).

The direct use of a liquid crystal as active spacer [19] needs the manufacture of a dedicated thin cell (typically 10 to 25 μm), constituted by two parallel glass substrates coated with all-dielectric mirror and transparent ITO electrodes. These driving electrodes are placed between the glass substrate and the mirror, in order to be located outside the resonator. The thin cell is filled with the nematic liquid crystal material, the VAN (Vertically Aligned Nematic) and PAN (Parallel Aligned Nematic) configurations being preferred to the TN one (Twisted Nematic), even if their polarization dependence is more marked. Large tuning range can be achieved (up to 80 nm), with relatively low insertion losses (-5 dB for a single cavity).

It is also possible to incorporate the liquid crystal as a dispersed phase in a polymer host (n-PDLC, for nano-phase polymer dispersed liquid crystal material) and to use the same cavity design as above, the filling of the cell being replaced by a casting of the precursor mixtures between the two coated glass substrates [20]. The tuning of the cavity is achieved again through a change in the voltage applied on the ITO electrodes, the experimental sensitivity being equivalent to an effective electro-optic constant of 700 pm/V at 1550 nm (to compare to 30 pm/V for the lithium niobate). Experimental results show an extra-influence of the applied voltage on the maximum transmittance of the cavity, because the refractive index change of the dispersed phase induced by the electric field can modify the scatter losses level in the n-PDLC). As for the previous design, a thermal stabilization of the filter response shall be implemented, to overcome the significant thermo-optic effect in polymers and liquid crystals: this can be achieved for instance, through a high frequency (typically 50 kHz) dedicated driving voltage.

6. CONCLUSION

A comparative analysis of the different mechanisms which can be used to tune a narrow-bandpass thin-film filter has been presented. Beside classical devices using rotation or translation mechanisms, new completely static systems with attractive features appear, especially based on the thermo-optic effect in semiconductor materials manufactured by PECVD and on the development of active solid-spaced etalons.

REFERENCES

1. P. Duggan, M. Tremblay, N. Rowhani and M. S. Ner, *Tunable filters provide flexibility for agile networks*, WDM Solutions, 9-12 (February 2003)
2. M. Lequime, R. Parmentier, F. Lemarchand and C. Amra, *Toward tunable thin-film filters for wavelength division multiplexing applications*, Appl. Opt. **41**, 3277-3284 (2002)
3. C. R. Pidgeon and S. D. Smith, *Resolving power of multilayer filters in non-parallel light*, J. Opt. Soc. Am. **54**, 1459-1466 (1964)
4. H. A. Macleod, *Thin-Film Optical Filters (3rd Edition)*, Philadelphia, Institute of Physics Publishing (2001)

5. MICRON OPTICS Chameleon Thin-Film Tunable Filter CTF-TF, http://www.micronoptics.com/pdfs/CTF-TF.pdf
6. Ph. Baumeister, *Optical Coating Technology*, section 9.5.9, *Masking to produce a non uniform distribution* (2001)
7. SANTEC Programmable Optical Tunable Filter OTF-920, http://www.santec.com/pdf/lasers/OTF-920.pdf
8. H. Takashashi, *Temperature stability of thin-film narrow-bandpass filters produced by ion-assisted deposition*, Appl. Opt. **34**, 667-675 (1995)
9. R. Parmentier and M. Lequime, *Substrate-strain-induced tunability of dense wavelength-division multiplexing thin-film filters*, Opt. Lett. **28**, 728-730 and 1279 (2003)
10. SCHOTT DWDM Filter Substrates, http://www.schott.com/optics_devices/english/products/dwdm.html
11. OHARA Negative Thermal Expansion Glass-ceramics NEX http://www.ohara-inc.co.jp/b/b02/b0214_ne/b0214.htm
12. M. Zgonik, P. Bernasconi, M. Duelli, R. Schlesser, P. Günter, M. H. Garrett, D. Rytz, Y. Zhu and X. Wu, *Dielectric, elastic, piezoelectric, electro-optic and elasto-optic tensors of BaTiO3 crystals*, Phys. Rev. B **50**, 5941-5949 (1994)
13. L. Domash, E. Ma, R. Murano, N. Nemchuk, A. Payne, S. Sherman, M. Wagner and M. Wu, International Patent WO 02/103441 (2002)
14. R. Parmentier, F. Lemarchand, M. Cathelinaud, M. Lequime and C. Amra, *Piezoelectric tantalum pentoxide studied for optical tunable applications*, Appl. Opt. **34**, 3270-3276 (2002)
15. J. Floriot, F. Lemarchand and M. Lequime, *Double Coherent Solid-spaced Filters for very narrow-bandpass filtering applications*, Opt. Commun. **222**, 101 (2003)
16. R. Parmentier, *Filtre interférentiel à bande étroite accordable – Principes de base et application au secteur des télécommunications optiques*, Thesis document, Université Aix-Marseille III (2002)
17. L. Domash, E. Ma, N. Nemchuk, A. Payne and M. Wu, *Tunable Thin Film Filters*, Paper ThM3, OFC 2003
18. L. Domash, M. Wu, N. Nemchuk and R. Murano, *Switchable thin film add/drop filter*, Post-deadline Paper PD35, OFC 2003
19. W. Vogel and M. Berroth, *Tuneable liquid crystal Fabry-Perot filters*, Proceedings of SPIE **4944**, 293-302 (2003)
20. K. Lewis, G. Smith, I. Mason and K. Rochester, *Design Issues for Tunable Filters for Optical Telecommunications*, Proceedings of SPIE **4679**, 213-223 (2002)